Evolution to a smooth universe in an ekpyrotic contracting phase with $w > 1$

David Garfinkle,[1,*] Woei Chet Lim,[2,+] Frans Pretorius,[2,‡] and Paul J. Steinhardt[2,3,§]

[1]*Department of Physics, Oakland University, Rochester, Michigan 48309, USA*
[2]*Joseph Henry Laboratories, Princeton University, Princeton, New Jersey 08544, USA*
[3]*Princeton Center for Theoretical Science, Princeton University, Princeton, New Jersey 08544, USA*

(Received 6 August 2008; published 27 October 2008)

A period of slow contraction with equation of state $w > 1$, known as an ekpyrotic phase, has been shown to flatten and smooth the universe if it begins the phase with small perturbations. In this paper, we explore how robust and powerful the ekpyrotic smoothing mechanism is by beginning with highly inhomogeneous and anisotropic initial conditions and numerically solving for the subsequent evolution of the universe. Our studies, based on a universe with gravity plus a scalar field with a negative exponential potential, show that some regions become homogeneous and isotropic while others exhibit inhomogeneous and anisotropic behavior in which the scalar field behaves like a fluid with $w = 1$. We find that the ekpyrotic smoothing mechanism is robust in the sense that the ratio of the proper volume of the smooth to nonsmooth region grows exponentially fast along time slices of constant mean curvature.

DOI: 10.1103/PhysRevD.78.083537 PACS numbers: 98.80.Cq

I. INTRODUCTION

For over two decades, the only known mechanism for homogenizing, isotropizing, and flattening the universe was inflation, a period of accelerated expansion with an equation of state w (ratio of pressure to energy density) near -1. Its success in resolving the horizon and flatness problems is a principal reason why inflation became an essential part of the standard model of cosmology. In recent years, an alternative mechanism has been discovered in which smoothing and flattening occurs before the big bang as the universe undergoes a period of slow contraction with $w > 1$. This alternative, known as the ekpyrotic mechanism [1,2], has been incorporated in alternatives to standard big bang inflationary cosmology including the "ekpyrotic" [1], "new ekpyrotic" [3], and cyclic models [4]. We note that both the inflationary and ekpyrotic mechanisms can produce nearly scale-invariant spectra for density perturbations in addition to smoothing and flattening the universe.

Until now, the ekpyrotic mechanism has only been shown to work in cases where the deviations from smoothness and flatness are small and perturbative when the ekpyrotic phase begins. The purpose of this paper is to show that the ekpyrotic mechanism is powerful and robust enough to smooth the universe even when the initial perturbations are large and nonlinear.

Let us first review how the inflation and the ekpyrotic mechanisms work in the perturbative regime where the cosmic evolution is well approximated by the Friedmann equation with an anisotropy term:

$$H^2 = \frac{8\pi G}{3}\left(\frac{\rho_m^0}{a^3} + \frac{\rho_r^0}{a^4} + \frac{\rho_w^0}{a^{3(1+w)}}\right) - \frac{k}{a^2} + \frac{\sigma^2}{a^6}, \quad (1)$$

where $H \equiv \dot{a}/a$ is the Hubble parameter; $a(t)$ is the Friedmann-Robertson-Walker (FRW) scale factor normalized so that the value today, t_0, is $a(t_0) = 1$; ρ_i^0 represents the present value of the energy density for component i, where m represents nonrelativistic matter, r represents radiation, and w represents an energy component with equation of state w, such as a scalar field and its potential. The last two terms on the right-hand side represent spatial curvature and anisotropy.

For an expanding universe, the term that dominates Eq. (1) after a long period of expansion is the one with the smallest power of a in the denominator. With only radiation and matter, the dominant term would be the spatial curvature, leading to a universe that is unacceptably open or closed by the present epoch. However, introducing an energy component with $w \approx -1$ totally changes the outcome because this component (ρ_w) then has the smallest exponent and dominates the Einstein equation, while the curvature and anisotropy (and other energy components) become negligible. This is the essence of how inflation works if the initial conditions are perturbative. For inflation, there are several "cosmic no-hair" theorems in addition to numerical results supporting the claim that homogeneity, isotropy, and flatness develop even when the initial conditions are nonlinear and nonperturbative [5,6].

Now consider the analogous arguments for a contracting universe. With $a(t)$ shrinking, the dominant term in Eq. (1) will be the one with the largest exponent of a in the denominator. For a universe with matter and radiation only, this would be the anisotropy term, which famously overtakes the evolution and drives the universe into chaotic mixmaster behavior. On the other hand, if there is an energy component with $w > +1$, then this energy compo-

*garfinkl@oakland.edu
+wlim@princeton.edu
‡fpretori@princeton.edu
§steinh@princeton.edu

nent dominates instead of anisotropy or spatial curvature, and chaotic mixmaster behavior never begins [2]. For a scalar field ϕ with potential energy density $V(\phi)$, the ratio of pressure to energy density is

$$w \equiv \frac{\frac{1}{2}\dot{\phi}^2 - V}{\frac{1}{2}\dot{\phi}^2 + V}, \tag{2}$$

which can be significantly greater than unity when V is less than zero and non-negligible, and which approaches $w = 1$ if the scalar field kinetic energy dominates. The ekpyrotic phase in ekpyrotic and cyclic models includes an effective scalar field component of this type.

For the cyclic model, the ekpyrotic phase is preceded by a period of dark energy domination and accelerated expansion which, if sustained long enough, would make the universe uniform and flat before the ekpyrotic contraction phase begins. In this case, the perturbative argument above should be reliable and sufficient to conclude that the universe is smooth and flat as it approaches the big crunch. However, in the ekpyrotic or new ekpyrotic models, generally, or in the cyclic model with a very short dark energy phase, the conditions at the beginning of the ekpyrotic phase are under less control.

This paper investigates the robustness of the ekpyrotic smoothing and flattening mechanism when the initial conditions are nonlinear and nonperturbative to determine how the situation compares with the perturbative case and with inflation. For this study we are not concerned with any particular form for the initial conditions that may be motivated by some specific model; rather, we would like to understand how a generic, highly inhomogeneous and anisotropic spacetime evolves under the influence of the proposed smoothing mechanism, modeled here by a scalar field with a negative exponential potential. Such negative exponential potentials arise naturally in supergravity and in string theory. Investigation of the proposed smoothing mechanism requires numerical solution of the coupled Einstein-scalar system of equations. For simplicity, we restrict our studies to deviations from smoothness along a single spatial dimension.

We use an orthonormal frame representation of the equations written in terms of Hubble-normalized, scale-invariant variables [7] similar to that described in [8], though here coupling to a scalar field instead of a fluid, and using constant-mean-curvature (CMC) time slices. We discretize the equations using second-order accurate finite difference techniques, and solve them with a variant of the Berger and Oliger [9] adaptive mesh refinement (AMR) algorithm for coupled elliptic-hyperbolic equations [10]. We find smooth regions that are scalar field dominated in which the scalar field (kinetic plus potential energy density) component behaves like a fluid with $w \gg 1$, and also regions where the scalar field kinetic energy dominates over the potential energy and the scalar field behaves like a fluid with $w = 1$. These latter regions remain inhomogeneous and anisotropic, and throughout this paper we will refer to these parts of the universe as the "anisotropic regions." Note however that the anisotropic regions are neither anisotropy nor matter dominated because both the scalar field and the anisotropy of the metric play important roles in the dynamics. Futhermore, note that despite the fact that matter in the smooth regions behaves effectively like a fluid with $w \gg 1$, there is no issue of superluminal propagation as might arise from an actual fluid with such an equation of state. This is because we are always solving the scalar wave equation with potential where disturbances always propagate within the light cone. In the anisotropic regions "spikes" also form, which are places where the fields change on very small spatial scales, and are similar to regions with this property that have been observed in numerical simulations of singularities in vacuum spacetimes [11]. Despite the presence of the scalar field, the anisotropic regions exhibit dynamical behavior similar to chaotic mixmaster vacuum solutions, where there are a series of relatively quick transitions between longer epochs where the solution can be described by a $w = 1$ Bianchi type I spacetime. A difference here though is that there are only a *finite* number of transitions, so the mixmaster behavior terminates after several transitions. These dynamics are also known to occur in spacetimes where the matter *is* a fluid with $w = 1$ [8,12]. AMR is necessary to resolve the spiky features that form both in the anisotropic regions and, in some instances, briefly in what will eventually become smooth scalar field dominated regions, and to resolve the almost domain wall-like transitions that develop between the smooth and anisotropic regions.

The outline for the rest of the paper is as follows. In Sec. II we describe the equations, initial conditions, and numerical methods used to solve them. We present the results in Sec. III. The primary conclusion is that a scalar field with a potential inspired by cyclic models is a remarkably powerful and robust smoothing mechanism during a contracting phase of the universe, able to drive the spacetime to homogeneity and isostropy even starting with highly nonlinear deviations from a FRW spacetime. Concluding remarks and a discussion of future work are given in Sec. IV.

II. THE EQUATIONS AND SOLUTION METHOD

The method we use to evolve the Einstein-scalar equations is the scale-invariant tetrad method of Uggla *et al.* [7]. We use this method with constant-mean-curvature slicing as is done in the vacuum simulations of [13] but with scalar field matter instead of vacuum. Thus our system can be thought of as the system of [13] but with extra variables and equations describing the matter, and with extra source terms for the influence of the matter on the metric evolution equations. More information on this type of method can be found in [7,13].

The spacetime is described in terms of a coordinate system (t, x^i) and a tetrad $(\mathbf{e}_0, \mathbf{e}_\alpha)$ where both the spatial coordinate index i and the spatial tetrad index α go from 1 to 3. Choose $\mathbf{e}_0$ to be hypersurface orthogonal with the relation between the tetrad and coordinates of the form $\mathbf{e}_0 = N^{-1}\partial_t$, and $\mathbf{e}_\alpha = e_\alpha{}^i\partial_i$, where N is the lapse and the shift is chosen to be zero. Choose the spatial frame $\{\mathbf{e}_\alpha\}$ to be Fermi propagated along the integral curves of $\mathbf{e}_0$. The commutators of the tetrad components are decomposed as follows:

$$[\mathbf{e}_0, \mathbf{e}_\alpha] = \dot{u}_\alpha \mathbf{e}_0 - (H\delta_\alpha{}^\beta + \sigma_\alpha{}^\beta)\mathbf{e}_\beta, \tag{3}$$

$$[\mathbf{e}_\alpha, \mathbf{e}_\beta] = (2a_{[\alpha}\delta_{\beta]}{}^\gamma + \epsilon_{\alpha\beta\delta}n^{\delta\gamma})\mathbf{e}_\gamma, \tag{4}$$

where $n^{\alpha\beta}$ is symmetric, and $\sigma^{\alpha\beta}$ is symmetric and trace-free. The scale-invariant tetrad variables are defined by $\boldsymbol{\partial}_0 \equiv \mathbf{e}_0/H$ and $\boldsymbol{\partial}_\alpha \equiv \mathbf{e}_\alpha/H$ while scale-invariant versions of the other gravitational variables are given by

$$\{E_\alpha{}^i, \Sigma_{\alpha\beta}, A^\alpha, N_{\alpha\beta}\} \equiv \{e_\alpha{}^i, \sigma_{\alpha\beta}, a^\alpha, n_{\alpha\beta}\}/H. \tag{5}$$

Note that the relation between the scale-invariant tetrad variables and the coordinate derivatives is

$$\boldsymbol{\partial}_0 = \mathcal{N}^{-1}\partial_t, \tag{6}$$

$$\boldsymbol{\partial}_\alpha = E_\alpha{}^i\partial_i, \tag{7}$$

where $\mathcal{N} = NH$ is the scale-invariant lapse. The matter model is a scalar field ϕ with potential V of the form

$$V(\phi) = -V_0 e^{-k\phi}, \tag{8}$$

where V_0 and k are positive constants. The scale-invariant matter variables are given by

$$W = \boldsymbol{\partial}_0\phi, \tag{9}$$

$$S_\alpha = \boldsymbol{\partial}_\alpha\phi, \tag{10}$$

$$\bar{V} = V/H^2. \tag{11}$$

The time coordinate t is chosen so that

$$e^{-t} = 3H. \tag{12}$$

Here we have used the scale invariance of the physical system to make both t and H dimensionless quantities. Note that Eq. (12) means that the surfaces of constant time are constant-mean-curvature surfaces. Note also that the singularity is approached as $t \to -\infty$.

Because of Eq. (12) the scale-invariant lapse satisfies an elliptic equation

$$-\boldsymbol{\partial}^\alpha\boldsymbol{\partial}_\alpha\mathcal{N} + 2A^\alpha\boldsymbol{\partial}_\alpha\mathcal{N} + \mathcal{N}(3 + \Sigma_{\alpha\beta}\Sigma^{\alpha\beta} + W^2 - \bar{V}) = 3. \tag{13}$$

The gravitational quantities $E_\alpha{}^i$, A_α, $N^{\alpha\beta}$, and $\Sigma_{\alpha\beta}$ satisfy the following hyperbolic evolution equations:

$$\partial_t E_\alpha{}^i = E_\alpha{}^i - \mathcal{N}(E_\alpha{}^i + \Sigma_\alpha{}^\beta E_\beta{}^i), \tag{14}$$

$$\partial_t A_\alpha = A_\alpha + \tfrac{1}{2}\Sigma_\alpha{}^\beta\boldsymbol{\partial}_\beta\mathcal{N} - \boldsymbol{\partial}_\alpha\mathcal{N} + \mathcal{N}(\tfrac{1}{2}\boldsymbol{\partial}_\beta\Sigma_\alpha{}^\beta - A_\alpha - \Sigma_\alpha{}^\beta A_\beta), \tag{15}$$

$$\partial_t N^{\alpha\beta} = N^{\alpha\beta} - \epsilon^{\gamma\delta(\alpha}\Sigma_\delta{}^{\beta)}\boldsymbol{\partial}_\gamma\mathcal{N} + \mathcal{N}(-N^{\alpha\beta} + 2N^{(\alpha}{}_\gamma\Sigma^{\beta)\gamma} - \epsilon^{\gamma\delta(\alpha}\boldsymbol{\partial}_\gamma\Sigma_\delta{}^{\beta)}), \tag{16}$$

$$\begin{aligned}\partial_t\Sigma_{\alpha\beta} = {} & \Sigma_{\alpha\beta} + \boldsymbol{\partial}_{\langle\alpha}\boldsymbol{\partial}_{\beta\rangle}\mathcal{N} + A_{\langle\alpha}\boldsymbol{\partial}_{\beta\rangle}\mathcal{N} \\ & + \epsilon_{\gamma\delta(\alpha}N_{\beta)}{}^\delta\boldsymbol{\partial}^\gamma\mathcal{N} + \mathcal{N}[-3\Sigma_{\alpha\beta} - \boldsymbol{\partial}_{\langle\alpha}A_{\beta\rangle} \\ & - 2N_{\langle\alpha}{}^\gamma N_{\beta\rangle\gamma} + N^\gamma{}_\gamma N_{\langle\alpha\beta\rangle} \\ & + \epsilon_{\gamma\delta(\alpha}(\boldsymbol{\partial}^\gamma N_{\beta)}{}^\delta - 2A^\gamma N_{\beta)}{}^\delta) + S_{\langle\alpha}S_{\beta\rangle}].\end{aligned} \tag{17}$$

Here parentheses around a pair of indices denote the symmetric part, while angle brackets denote the symmetric trace-free part.

The equations of motion for the matter variables are as follows:

$$\partial_t\phi = \mathcal{N}W, \tag{18}$$

$$\partial_t S_\alpha = S_\alpha + W\boldsymbol{\partial}_\alpha\mathcal{N} + \mathcal{N}[\boldsymbol{\partial}_\alpha W - (S_\alpha + \Sigma_\alpha{}^\beta S_\beta)], \tag{19}$$

$$\partial_t W = W + S^\alpha\boldsymbol{\partial}_\alpha\mathcal{N} + \mathcal{N}\left(\boldsymbol{\partial}^\alpha S_\alpha - 3W - 2A^\alpha S_\alpha - \frac{\partial\bar{V}}{\partial\phi}\right). \tag{20}$$

In addition, the variables are subject to the vanishing of the following constraint quantities:

$$(\mathcal{C}_{\mathrm{com}})^{\lambda i} = \epsilon^{\alpha\beta\lambda}[\boldsymbol{\partial}_\alpha E_\beta{}^i - A_\alpha E_\beta{}^i] - N^{\lambda\gamma}E_\gamma{}^i, \tag{21}$$

$$(\mathcal{C}_J)^\gamma = \boldsymbol{\partial}_\alpha N^{\alpha\gamma} + \epsilon^{\alpha\beta\gamma}\partial_\alpha A_\beta - 2A_\alpha N^{\alpha\gamma}, \tag{22}$$

$$(\mathcal{C}_C)_\alpha = \boldsymbol{\partial}_\beta\Sigma_\alpha{}^\beta - 3\Sigma_\alpha{}^\beta A_\beta - \epsilon_{\alpha\beta\gamma}N^{\beta\delta}\Sigma_\delta{}^\gamma - WS_\alpha, \tag{23}$$

$$\mathcal{C}_G = 1 + \frac{2}{3}\boldsymbol{\partial}_\alpha A^\alpha - A^\alpha A_\alpha - \frac{1}{6}N^{\alpha\beta}N_{\alpha\beta} + \frac{1}{12}(N^\gamma{}_\gamma)^2 - \frac{1}{6}\Sigma^{\alpha\beta}\Sigma_{\alpha\beta} - \frac{1}{6}W^2 - \frac{1}{6}S^\alpha S_\alpha - \frac{1}{3}\bar{V}, \tag{24}$$

$$(\mathcal{C}_S)_\alpha = S_\alpha - \boldsymbol{\partial}_\alpha\phi. \tag{25}$$

The evolution equations can be freely modified by adding multiples of the constraints to them. In particular, for numerical stability we add a multiple of $(\mathcal{C}_C)_\alpha$ to the right-hand side of the evolution equation for A_α [14].

The initial data must be chosen so that the constraint equations are satisfied, and then the evolution equations

will ensure that they remain satisfied. We find solutions of the constraint equations essentially the same way as is done for more standard methods of numerical relativity: by using the York method [15]. That is, we choose certain components of the variables and then solve the constraints for the rest. Our choice is by no means the most general one possible; but it is general enough that we expect any behavior that emerges from the evolution of these data to reflect the general behavior of singularities for this type of matter. This expectation is bolstered by the experience of numerical simulations of vacuum singularities. In particular, the greatest restriction on the generality of our initial data comes from the fact that we restrict our studies to deviations in homogeneity along a single spatial direction. Our spacetimes thus have two Killing fields. Nonetheless we choose our initial data to be the sort that, in the vacuum two Killing field case [16], were sufficiently general that the behavior as the singularity was approached was the same as that of more general initial data in the case with no symmetries [17].

In the usual approach to numerical relativity the initial data consist of the spatial metric and the extrinsic curvature. The York method then involves choosing a metric conformally related to the spatial metric and part of a tensor conformally related to the extrinsic curvature, and then solving for the conformal factor ψ as well as the rest of the extrinsic curvature. Since we are using a tetrad approach, we must also have an initial spatial triad consistent with the initial spatial metric. For simplicity, we choose the initial conformal metric to be flat and (x, y, z) to be the usual Cartesian coordinates for that metric, and we choose the spatial triad to lie along those spatial directions. Thus, the scale-free spatial triad becomes

$$E_\alpha{}^i = H^{-1}\psi^{-2}\delta_\alpha{}^i. \tag{26}$$

It then follows from Eq. (4) that

$$A_\alpha = -2\psi^{-1}E_\alpha{}^i\partial_i\psi, \tag{27}$$

$$N_{\alpha\beta} = 0. \tag{28}$$

The shear is essentially the trace-free part of the extrinsic curvature, and as in the usual approach in numerical relativity, the constraint equations simplify for a particular rescaling of the trace-free part of the extrinsic curvature with the conformal factor. We therefore introduce the quantity $Z_{\alpha\beta}$ defined by

$$\Sigma_{\alpha\beta} = \psi^{-6}Z_{\alpha\beta}. \tag{29}$$

Similar considerations apply to the matter variables, leading us to define the quantity Q given by

$$W = \psi^{-6}Q. \tag{30}$$

Here we will specify Q, ϕ and a part of Z_{ik} and solve the constraint equations for the conformal factor ψ and the rest of Z_{ik}. For convenience of the numerical simulations, we choose periodic boundary conditions $0 \le x \le 2\pi$ with 0 and 2π identified, where x is the single spatial coordinate that the metric and matter variables depend on. Also, identifying the other spatial coordinates y and z means that our simulation is of a spacetime with spatial topology T^3. Since the variables depend only on x and since x is periodically identified, specifying a variable means giving the coefficients of a Fourier expansion of that variable.

From Eq. (23) and our ansatz for the scale-invariant variables, we obtain

$$\partial^i Z_{ik} = Q\partial_k\phi. \tag{31}$$

In the vacuum case (i.e. for vanishing scalar field) this equation simply becomes the condition that Z_{ik} is divergence-free, which is in turn simply an algebraic condition on the Fourier coefficients of Z_{ik}. Note that since $\Sigma_{\alpha\beta}$ must be trace-free, so must Z_{ik}. A simple, but still fairly general divergence-free and trace-free Z_{ik} is the following:

$$Z_{ik} = \begin{pmatrix} b_2 & \xi & 0 \\ \xi & a_1\cos x + b_1 & a_2\cos x \\ 0 & a_2\cos x & -b_1 - b_2 - a_1\cos x \end{pmatrix}, \tag{32}$$

where ξ, a_1, a_2, b_1, and b_2 are constants. We still keep this divergence-free part of Z_{ik} but now add to it a piece that has a nonzero divergence. We simply specify the Fourier coefficients of ϕ and Q via

$$Q(x, t = 0) = \frac{f_1}{H}\cos(m_1 x + d_1), \tag{33}$$

$$\phi(x, t = 0) = f_2\cos(m_2 x + d_2), \tag{34}$$

where f_1, m_1, d_1, f_2, m_2, and d_2 are constants. This turns Eq. (31) into an algebraic equation for the Fourier coefficients of this nonzero divergence piece of Z_{ik} which we then solve.

Now imposing Eq. (24) our ansatz yields

$$\begin{aligned}\partial^i\partial_i\psi = {} & (\tfrac{3}{4}H^2 - \tfrac{1}{4}V)\psi^5 - \tfrac{1}{8}(\partial^i\phi\,\partial_i\phi)\psi \\ & - \tfrac{1}{8}(Q^2 + Z^{ik}Z_{ik})H^2\psi^{-7},\end{aligned} \tag{35}$$

which is solved for the conformal factor ψ using the numerical methods described below.

The constraint equations (21) and (22) are automatically satisfied by this ansatz. We then satisfy Eq. (25) by using the given value of ϕ to compute the initial value of S_α.

Numerical code

We discretize the system of equations described in the previous section using second-order accurate finite difference methods, with Berger and Oliger [9] style AMR as provided by the PAMR toolkit [18]. On a single grid a two-time level, Crank-Nicholson (CN)-like discretization scheme is used. Standard centered spatial derivative opera-

tors are employed, and in the hyperbolic evolution equations, spatial derivatives (and undifferentiated functions) are averaged over the two time levels as usual within a CN scheme. Kreiss-Oliger dissipation [19] is applied, and, although not necessary for the stability of unigrid evolutions, is important for reducing unphysical high-frequency solution components sometimes introduced at refinement boundaries. The elliptic equations are solved using a FAS (full-approximation-storage) multigrid algorithm [20].

The elliptic slicing condition is incorporated into the Berger and Oliger time-stepping algorithm using the method described in [10]. Such modifications are necessary to take advantage of time subcycling; however, here we find that we can evolve the system without time subcycling yet keep the time step equal to that of the *coarsest* level in the hierarchy. In other words, with a spatial refinement ratio of $\rho_{\rm sp}$ a given level L_i in the hierarchy (with level L_1 being the coarsest) will have a CFL (Courant-Friedrichs-Lewy) factor $\lambda_i = \Delta t_i/\Delta x_i = \Delta t_1/\Delta x_i$ equal to ${\rho_{\rm sp}}^{i-1}$ times that of the base level λ_1. In a typical simulation we use $\lambda_1 = 0.2$, $\rho_{\rm sp} = 2$, and have run cases where up to 25 levels of refinement were used, giving $\lambda_{25} \approx 3 \times 10^6$. Our code shows no signs of instability, and exhibits clear second-order convergence. Though technically the evolution scheme is implicit due to the CN differencing, at each time step the code is able to converge to a solution within several iterations at most. We surmise that this rather atypical behavior for the solution of hyperbolic difference equations is due to the ultralocal nature of the spacetime in the approach to the singularity [16,17]. This is reflected in the differential equations by the spatial derivative terms becoming negligible; hence, they are essentially reduced to a set of ordinary differential equations in time, one at each grid point in the domain.

III. RESULTS

We have run simulations for a variety of initial conditions; here we show results from a single example that demonstrates the generic behavior: evolution from a highly inhomogeneous, anisotropic universe with significant curvature at the initial time to a universe containing distinct volumes of either smooth, homogeneous $w \gg 1$ matter dominated regions, or $w = 1$ anisotropic regions. Whenever a $w \gg 1$ region forms it grows exponentially fast in proper volume relative to $w = 1$ regions.

The particular initial conditions for this example are [(32)–(34)]

$$a_1 = 0.70, \quad a_2 = 0.10, \quad \xi = 0.01,$$
$$b_1 = 1.80, \quad b_2 = -0.15, \quad f_1 = 2.00,$$
$$m_1 = 1, \quad d_1 = -1.7, \quad f_2 = 0.15,$$
$$m_2 = 2, \quad d_2 = -1.0,$$

and

$$V_0 = 0.1, \quad k = 10 \tag{36}$$

for the scalar field potential parameters (8). The same initial data were evolved with several resolutions to confirm second-order convergence; the highest resolution has 2049 points on the base level, and up to 12 additional levels of 2:1 refinement.

It is enlightening to visualize the evolution via the behavior of the matter (Ω_m), shear (Ω_s), and curvature (Ω_k) contributions to the normalized energy density, defined as

$$\Omega_m \equiv \tfrac{1}{6}W^2 + \tfrac{1}{6}S^\alpha S_\alpha + \tfrac{1}{3}\bar{V}, \tag{37}$$

$$\Omega_s \equiv \tfrac{1}{6}\Sigma^{\alpha\beta}\Sigma_{\alpha\beta}, \tag{38}$$

$$\Omega_k \equiv -\frac{2}{3}\partial_\alpha A^\alpha + A^\alpha A_\alpha + \frac{1}{6}N^{\alpha\beta}N_{\alpha\beta} - \frac{1}{12}(N^\gamma{}_\gamma)^2, \tag{39}$$

where $\Omega_m + \Omega_s + \Omega_k = 1$ by (24). Figure 1 shows these quantities plotted at select times during the evolution (which was stopped at $t = -150$). Note that all features in the solution are locally smooth—apparent step functions in some of the plots are simply due to the large size of the domain relative to the size of the feature. As an example, Fig. 2 shows a zoom-in of the last panel of Fig. 1 about one of the late-time spike structures that formed in the anisotropic regime.

The effective equation of state parameter w is shown in Fig. 3, which takes the following form in Hubble-

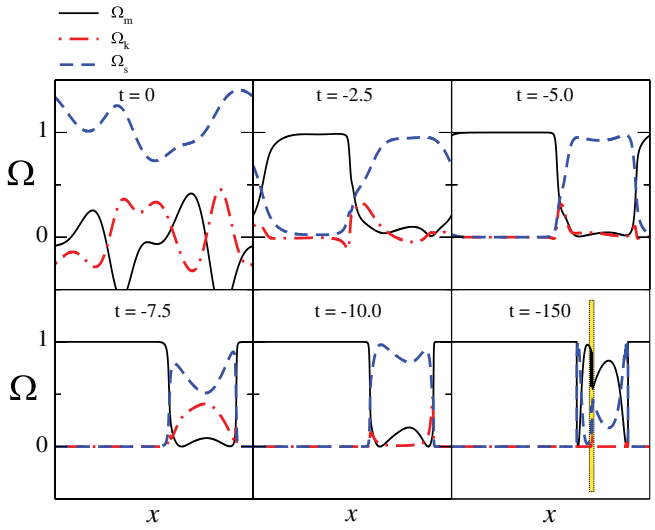

FIG. 1 (color online). $t = $ const snapshots of the normalized energy density in matter Ω_m (solid line), curvature Ω_k (dot-dash line), and shear Ω_s (dashed line) for $0 \le x \le 2\pi$ at several times during the evolution of the initial data described in Sec. III. Time runs from left to right along the top row and continues along the bottom row. The shaded slit (dotted outline) in the last panel ($t = -150$) indicates the range of x shown in the blowup in Fig. 2.

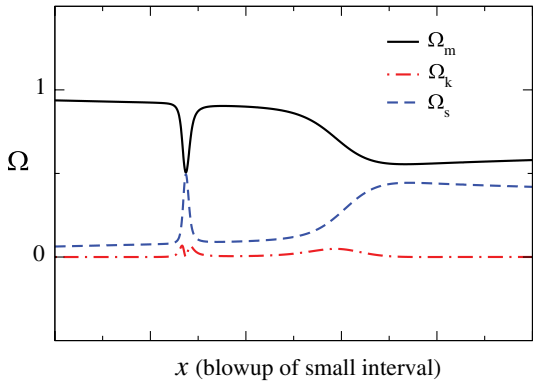

FIG. 2 (color online). Zooming in on one of the spike structures that formed in the anisotropic region at $t = -150$, as shown in Fig. 1.

normalized variables:

$$w = \frac{\frac{1}{2}W^2 + \frac{1}{2}S^\alpha S_\alpha - \bar{V}}{\frac{1}{2}W^2 + \frac{1}{2}S^\alpha S_\alpha + \bar{V}}. \tag{40}$$

By comparing Figs. 1 and 3 it is evident that at late times the region that has smoothed out and become matter dominated coincides with $w \gg 1$, whereas the anisotropic regime evolves to $w = 1$ (and exactly so to within numerical truncation error).

The asymptotic behavior of the spacetime in the matter dominated region appears to coincide with that of a spacetime with an isotropic singularity in the sense of Goode and Wainwright [21]. We therefore conjecture that in an ekpyrotic phase with an exponential potential, an open set of initial conditions leads to an isotropic singularity.

We can understand the behavior of the solution in the asymptotic matter dominated region by applying the following approximation which we expect to hold to arbitrary accuracy as the singularity is approached. To begin with, we neglect all spatial derivatives (such an approximation also holds in the anisotropic regions away from the isolated spikes). The constraint (24) then reduces to

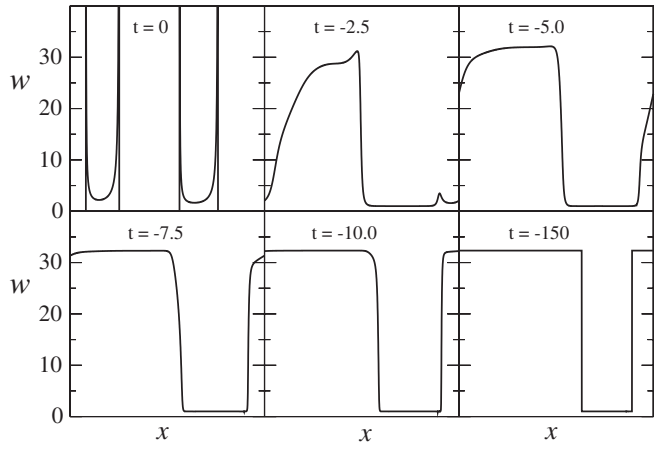

FIG. 3. The effective equation of state parameter w (40) for the simulation described in Sec. III, for $0 \le x \le 2\pi$ at the same times as in Fig. 1. At late times $w \to k^2/3 - 1$ in the matter dominated region, and $w \to 1$ in the anisotropic region [in this simulation $k = 10$ for the potential (8)].

$$\frac{W^2 + 2\bar{V}}{6} - 1 \approx 0, \tag{41}$$

and the slicing condition for $\mathcal{N}$ (13) becomes

$$3\mathcal{N} \approx \frac{3}{3 - \bar{V}}, \tag{42}$$

where we have used (41) to simplify the expression. We then assume that $\bar{V}$ remains finite and nonzero as the singularity is approached. This implies from (8), (11), and (12) that ϕ takes the asymptotic form

$$\phi(x, t) \approx \phi_0(x) + \frac{2t}{k} \tag{43}$$

where k is the constant in the expression for the potential $V = -V_0 \exp(-k\phi)$. Thus W (9) tends to

$$W \approx \frac{2}{k\mathcal{N}}. \tag{44}$$

Combining these relations gives

$$W \approx k, \tag{45}$$

$$\bar{V} \approx 3 - \frac{k^2}{2}, \tag{46}$$

$$\mathcal{N} \approx \frac{2}{k^2}, \tag{47}$$

and from (40)

$$w \approx k^2/3 - 1. \tag{48}$$

We conjecture that at the singularity the above approximations become exact, namely,

$$\lim_{t \to -\infty} W = k, \tag{49}$$

$$\lim_{t \to -\infty} \bar{V} = 3 - \frac{k^2}{2}, \tag{50}$$

$$\lim_{t \to -\infty} \mathcal{N} = \frac{2}{k^2}, \tag{51}$$

$$\lim_{t \to -\infty} w = k^2/3 - 1. \tag{52}$$

Our simulations support this conjecture in that at late times ($t = -150$ in this example) these quantities have, to within numerical truncation error, reached their limiting values. Detailed analysis of the asymptotic dynamics can be carried out following the method of [12,22,23].

Figure 3 shows that as the singularity is approached the *coordinate* volumes of the $w = 1$ vs $w \gg 1$ regions of the universe are comparable. However, it turns out that the ratio of the *proper* volume of matter to anisotropic regions grows exponentially with time. Let S denote the proper spatial volume element associated with the spatial metric h_{ij} of $t = \text{const}$ slices, i.e., $S = \sqrt{\det h}$. The fractional change of S with respect to time is

$$\partial_t \ln S = -\tfrac{1}{2} h_{ij} \partial_t h^{ij}, \tag{53}$$

which can be written as

$$\partial_t \ln S = 3\mathcal{N}. \tag{54}$$

Thus the scale-invariant lapse $\mathcal{N}$ is a direct measure of the rate at which the local proper volume element changes with time (and recall that $t \to -\infty$ as the singularity is approached). Figure 4 shows $3\mathcal{N}$ from the simulation at several times. In the asymptotic regime where spatial gradients are negligible, $\mathcal{N}$ approaches a constant (42), and thus (54) can be integrated to give

$$S_m \propto e^{6t/k^2}, \qquad w \gg 1, \tag{55}$$

$$S_v \propto e^{t}, \qquad w = 1, \tag{56}$$

where we have used (42) where $w \gg 1$, and note that $\bar{V} \approx 0$ when $w = 1$. Thus, at late times the ratio $\mathcal{R}$ of the proper volume of matter to anisotropic regions of the universe grows as

$$\mathcal{R} = \frac{\int S_m dx}{\int S_v dx} \propto e^{-t(1-6/k^2)}. \tag{57}$$

Thus, as long as $k > \sqrt{6}$ (which is equivalent to $w > 1$), $\mathcal{R} \to \infty$ as $t \to -\infty$.

Figure 5 shows five state space orbits projected onto the (Σ_+, Σ_-) plane, where

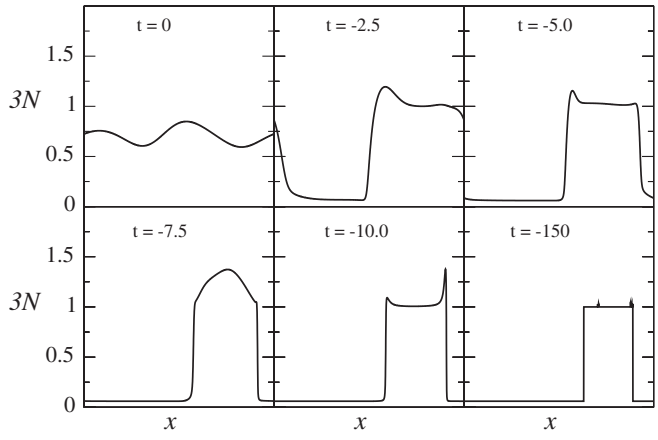

FIG. 4. Three times the scale-invariant lapse $\mathcal{N}$ for the simulation described in Sec. III, for $0 \le x \le 2\pi$ at the same output times as Figs. 1 and 2.

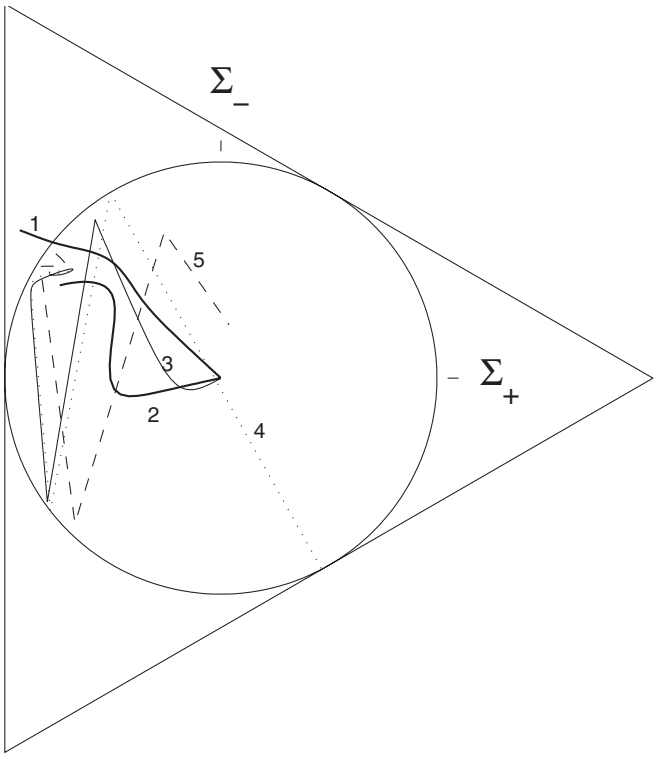

FIG. 5. The state space orbits for worldlines at $x = 0$, 3.0, 3.9, 4.0, 4.4. Towards the singularity, the first three orbits (solid lines) approach the origin of the plane, indicating isotropization. The fourth (dotted line) and the fifth (dashed line) do not isotropize.

$$\Sigma_+ = \frac{1}{2}(\Sigma_{11} + \Sigma_{22}), \qquad \Sigma_- = \frac{1}{2\sqrt{3}}(\Sigma_{11} - \Sigma_{22}). \tag{58}$$

The orbits correspond to the evolution along the worldlines at $x = 0$, 3.0, 3.9, 4.0, 4.4. All five orbits begin in the upper left quadrant, away from the origin, indicating anisotropic initial data. Towards the singularity, the first three orbits (solid lines) approach the origin of the plane, indicating isotropization. The fourth (dotted line) and the fifth (dashed line) do not isotropize.

IV. CONCLUSIONS

Our computations provide evidence that the ekpyrotic mechanism for smoothing and flattening the universe is robust and powerful, comparable qualitatively and quantitatively to the inflationary mechanism incorporated in the conventional big bang model. This evidence is the behavior, as the singularity is approached, of a class of spacetimes that, while not completely general, contain several degrees of freedom and begin far from FRW spacetime. Both the inflationary and the ekpyrotic mechanisms require the addition of an energy component that is commonly mocked up as a scalar field with potential energy. For inflation, the important feature is that, for some initial conditions, the scalar field can act like a fluid with $w \approx -1$. It has been shown numerically that, beginning from

highly nonlinear and highly irregular initial conditions, regions dominated by the scalar field and with $w \approx -1$ come to dominate the volume of the universe [6]. Similarly, we have found that the regions in which the scalar field acts like a fluid with $w > 1$ come to dominate the volume of the universe during a contracting phase.

This result addresses one of the key criticisms raised when the ekpyrotic model of the universe was first introduced; namely, it was suggested that the model required smooth initial conditions [24]. One of the motivations for extending the ekpyrotic picture into a cyclic model was to include a period of dark energy domination before the ekpyrotic phase began in order to prepare smooth conditions [4]. Now, from the results here, it is clear that the dark energy epoch is not required for this purpose. Not only does this allow the possibility that the dark energy phase lasts only a few e-folds in the cyclic picture, as suggested in [25], but it also opens the way for more general bouncing cosmologies that incorporate the ekpyrotic mechanism but do not cycle.

With these results in hand, we are now prepared to tackle the bounce itself in the case that it is nonsingular [$a(t)$ shrinks to a nonzero value and then begins to increase]. For the nonsingular bounce, the equation of state must decrease from $w > 1$ to $w < -1$ for a finite period during which anisotropy and inhomogeneity grow. Our goal is to determine if their growth can be kept at a level consistent with observations, establishing the viability of these bouncing cosmological models.

ACKNOWLEDGMENTS

This work is supported in part by the U.S. Department of Energy Grant No. DE-FG02-91ER40671 (P. J. S.), by NSF Grant No. PHY-0456655 (D. G.), by the Alfred P. Sloan Foundation (F. P.), and by NSF Grant No. PHY-0745779 (F. P.). Some computations were run on the Woodhen cluster at the Princeton Institute for Computational Science and Engineering (PICSciE).

[1] J. Khoury, B. A. Ovrut, P. J. Steinhardt, and N. Turok, Phys. Rev. D **64**, 123522 (2001).
[2] J. K. Erickson, D. H. Wesley, P. J. Steinhardt, and N. Turok, Phys. Rev. D **69**, 063514 (2004).
[3] E. I. Buchbinder, J. Khoury, and B. A. Ovrut, Phys. Rev. D **76**, 123503 (2007).
[4] P. J. Steinhardt and N. Turok, Science **296**, 1436 (2002).
[5] See, for example, Sec. 8.6 of E. Kolb and M. S. Turner, *The Early Universe* (Addison-Wesley, Redwood City, CA, 1994).
[6] D. S. Goldwirth, Phys. Rev. D **43**, 3204 (1991).
[7] C. Uggla, H. van Elst, J. Wainwright, and G. F. R. Ellis, Phys. Rev. D **68**, 103502 (2003).
[8] J. Curtis and D. Garfinkle, Phys. Rev. D **72**, 064003 (2005).
[9] M. J. Berger and J. Oliger, J. Comput. Phys. **53**, 484 (1984).
[10] F. Pretorius and M. W. Choptuik, J. Comput. Phys. **218**, 246 (2006).
[11] D. Garfinkle, Classical Quantum Gravity **21**, S219 (2004).
[12] A. A. Coley and W. C. Lim, Classical Quantum Gravity **22**, 3073 (2005).
[13] D. Garfinkle, Classical Quantum Gravity **24**, S295 (2007).
[14] D. Garfinkle and C. Gundlach, Classical Quantum Gravity **22**, 2679 (2005).
[15] J. W. York, Phys. Rev. Lett. **26**, 1656 (1971).
[16] B. K. Berger, D. Garfinkle, J. Isenberg, V. Moncrief, and M. Weaver, Mod. Phys. Lett. A **13**, 1565 (1998).
[17] D. Garfinkle, Phys. Rev. Lett. **93**, 161101 (2004).
[18] PAMR (Parallel Adaptive Mesh Refinement) and AMRD (Adaptive Mesh Refinement Driver) libraries (http://laplace.physics.ubc.ca/Group/Software.html).
[19] H. Kreiss and J. Oliger, *Global Atmospheric Research Programme*, Publications Series No. 10 (WMO-ICSU Joint Organization Committee, 1973).
[20] A. Brandt, Math. Comput. **31**, 333 (1977).
[21] S. W. Goode and J. Wainwright, Classical Quantum Gravity **2**, 99 (1985).
[22] W. C. Lim, H. van Elst, C. Uggla, and J. Wainwright, Phys. Rev. D **69**, 103507 (2004).
[23] A. A. Coley, Y. He, and W. C. Lim, Classical Quantum Gravity **21**, 1311 (2004).
[24] R. Kallosh, L. Kofman, and A. D. Linde, Phys. Rev. D **64**, 123523 (2001).
[25] J. K. Erickson, S. Gratton, P. J. Steinhardt, and N. Turok, Phys. Rev. D **75**, 123507 (2007).